Using coherent dynamics to quantify spin coupling within triplet-exciton/polaron complexes in organic diodes

W. J. Baker, T. L. Keevers, C. Boehme, and D. R. McCamey

Phys. Rev. B **92**, 041201 — Published 2 July 2015

DOI: 10.1103/PhysRevB.92.041201

Using coherent dynamics to quantify spin-coupling within triplet-exciton/polaron complexes in organic diodes

W. J. Baker,[1,2,3] T. L. Keevers,[1] C. Boehme,[3] and D. R. McCamey[1,*]

[1]*School of Physics, UNSW, Sydney NSW 2052, Australia*
[2]*Centre for Quantum Computation and Communication Technology, UNSW, Sydney NSW 2052, Australia*
[3]*Department of Physics and Astronomy, University of Utah, Salt Lake City, UT 84112*

(Dated: June 9, 2015)

Quantifying the spin-spin interactions which influence electronic transitions in organic semiconductors is crucial for understanding their magneto-optoelectronic properties. By combining a theoretical model for three spin interactions in the coherent regime with pulsed electrically detected magnetic resonance experiments on MEH-PPV diodes, we quantify the spin-coupling within complexes comprising three spin-1/2 particles. We determine that these particles form triplet-exciton/polaron pairs, where the polaron–exciton exchange is over 5 orders of magnitude weaker ($<$ 170 MHz) than that within the exciton. This approach provides a direct spectroscopic approach for distinguishing between coupling regimes, and to test hypotheses relating microscopic properties to bulk characteristics of organic electronic devices.

Spin–spin interactions between charge carriers in organic semiconductors mediate spin–dependent electronic processes such as recombination and transport. Quantifying these interactions is therefore crucial for understanding the macroscopic magneto–optoelectronic properties of these materials and devices made from them[1–4].

Pulsed electrically detected magnetic resonance (pEDMR) allows the observation of coherent spin motion during the application of a magnetic resonant excitation of charge carrier spins, providing a direct probe of interactions between spin systems which directly influence a materials conductivity. It has been used to quantify exchange and hyperfine interactions between recombining polaron pairs[5] as well as between polaron pairs and hydrogen nuclear spins[6,7]. Here, we focus for the first time on the application of pEDMR to interactions involving more than two spins. In particular, we aim to quantify the coupling of the three spin-1/2 particles involved in the recombination process mediated by triplet exciton-polaron (TEP) interactions. In recent years, the TEP model has been invoked to successfully explain magnetoresistance in organic semiconductors[8–10]. However, due to the ambiguity of linking magneto-optoelectronic materials properties with their underlying spin–dependent processes, spectroscopic confirmation of any claimed microscopic process is necessary[4]. This is especially true for experimental conditions where alternative spin-coupled states[11] and associated spin-dependent process can exist.

We previously demonstrated that pEDMR could be used to observe the TEP process in experiments on π-conjugated polymer poly[2-methoxy-5-(2-ethylhexyloxy)-1,4-phenylenevinylene] (MEH-PPV) based thin–film organic light-emitting diodes (OLEDs)[13].The study presented here provides a more detailed experimental and theoretical investigation of pEDMR on three-spin complexes to quantify the magnitude of the spin-spin couplings within them. Many quantitatively different coupling regimes are possible (see eg Ref[13]), with a correspondingly large number of theoretical proposals for their impact on the bulk magneto-conductive and magneto-optical process of organic devices. This work provides the experimental evidence required to distinguish between these hypotheses by directly measuring spin-spin coupling constants in three spin-1/2 systems.

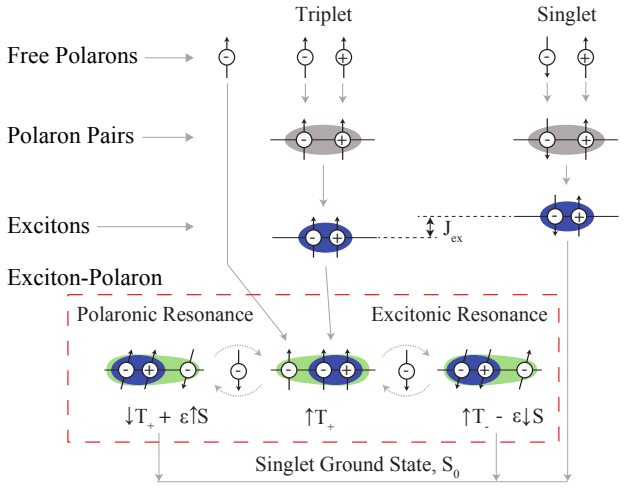

FIG. 1. Illustration of the TEP mechanism and how it influences conductivity when an ESR excitation takes place. Coulombically coupled electron and hole polaron pairs randomly recombine into excitonic states. Thereafter, the long–lived triplet excitons (TE) can interact with polarons forming TEP pairs - the focus of this study. The eigenstates of TE and polarons are mixed by the weak exchange and dipolar interactions between the polaron and exciton along with the intra-excitonic coupling, depicted here as ϵ. As a result, pulsed electron paramagnetic resonance (pEPR) on the TEP states can modify singlet content and thus the TEP recombination and sample conductivity can change.

Figure 1 depicts a hierarchy of spin configurations in an organic semiconductor under charge carrier injection, including TEP states. From the continuum of injected free charge carriers, weakly spin interacting polaron-pairs form[14,15], which can either dissociate or recombine via the excitonic states. Due to the singlet nature of the ground state and the requirements of spin–conservation, singlet-excitons can recombine directly while triplet-excitons require further interaction with the environment which causes them to exhibit longer lifetimes. The

TEP process requires triplet-excitons to interact with excess charge carriers to create triplet–exciton polaron complexes (see Fig.1). As proposed by Ern and Merrifield, the exciton relaxes to the ground state non-radiatively, transferring its excess energy to the (subsequently free) polaron, changing the conductivity in the device. Since this Auger-like recombination transition is dependent on the spin state of the three $s = 1/2$ manifold, it can be controlled directly with electron spin resonance (ESR), either via the polaronic or the excitonic resonance (Fig.1), and detected by monitoring the conductivity of the sample.

Figure 2(a) shows the eight spin eigenstates of a three $s = 1/2$ complex with strong exchange coupling J_{ex} and strong magnetic dipolar interaction D_{ex} between two of the three electron spins as a function of an externally applied magnetic field. The two strongly coupled spins form an exciton state with $s = 1$ which is then coupled through much weaker exchange coupling J_i to the remaining electron spin. J_i represents the individual exchange interaction between the free polaron and one of the carriers within the exciton. Our analysis shows that the frequency of nutation between the spin eigenstates under spin resonant excitation is governed by the sum of the two J_i terms, J_Σ. A small difference in the J_i terms ΔJ is needed to provide an observable change in recombination rate. Details of this analysis can be found in Ref. 16, along with calculations of the energies of these spin eigenstates displayed in Fig. 2a). At zero magnetic field, the energy is dominated by J_{ex} leaving the singlet manifold ≈ 0.7 eV = 170 THz[17] higher than the triplet exciton.

For the case of negligible spin interaction between the exciton and the polaron, the eigenstates are well approximated by the product basis of the $s = 1$ and $s = 1/2$ eigenstates (Fig.2 b, left column) where $\Delta J = 0$. However, when $\Delta J \neq 0$ (Fig.2 b, right column), the presence of the additional polaron causes a mixing of the triplet spin eigenstates, except for the $|\uparrow\rangle \otimes |T_+\rangle$ and $|\downarrow\rangle \otimes |T_-\rangle$ states. It is this mixture which causes the TEP recombination rate to depend on the occupation densities of spin–eigenstates and to therefore change when these densities are changed by magnetic resonant spin manipulation. Figure2 a) shows ESR–allowed spin transitions between eigenstates 3-4 and 6-8 in the presence of a magnetic field that will be referred to as the high–field resonance in the following, and between eigenstates 4-8 and 3-6 for what will be referred to as the low–field resonance. As the solutions of the TEP product states in Fig. 2(b)m as long as $\Delta J = 0$, the excitation of ESR–allowed transitions does not change the triplet content of the excited exciton states and thus, pEDMR signals do not exist[16].

When $\Delta J \neq 0$ and a sufficiently large and constant bias is applied to an MEH-PPV device with unbalanced injection, the TEP process will generate a surplus of $|\uparrow\rangle \otimes |T_+\rangle$ and $|\downarrow\rangle \otimes |T_-\rangle$ states. This is caused by the longer lifetimes of these states compared to all other eigenstates. The excitation of transitions 8-6 and 3-4 from the steady state will then increase the singlet-exciton content of the TEP ensemble, causing a measurable change of the recombination rate and the sample conductivity. A similar argument can be made for transitions 3-6 and 4-8 which can be excited under half–field conditions.

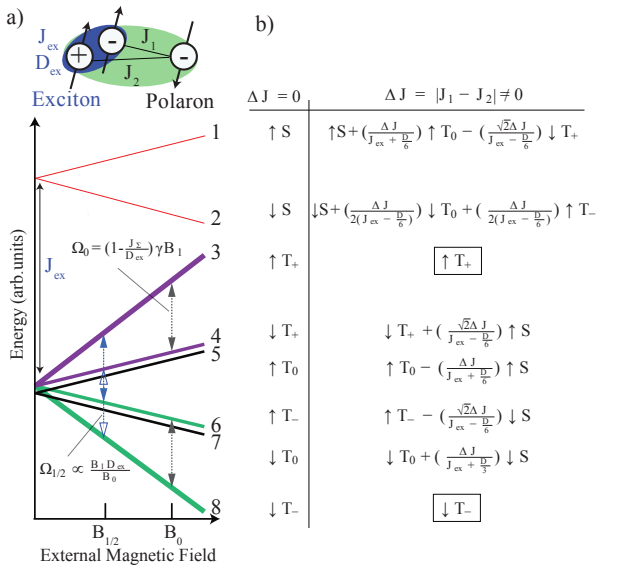

FIG. 2. Depiction of weakly spin–spin coupled exciton/polaron states with $\Delta J < J_\Sigma \ll J_{ex}, D_{ex}$). a) The energy term diagram of the eight spin eigenstates as a function of the applied external magnetic field B_0 with the arrows showing the ESR allowed transitions at full and half field conditions. Notice the separation in spin states at full-field governed by J_Σ (see text). b) Only when the small spin-coupling interaction between the exciton and polaron is non-vanishing ($\Delta J \neq 0$), a mixture of the exciton singlet and triplet–states occurs. Thus, only when $\Delta J \neq 0$, ESR can induced a change of the TEP recombination rate and therefore cause a pEDMR signal. The two states surrounded by boxes represent the dominantly occupied states under steady state device conditions before an ESR excitation takes place.

For the pEDMR experiments described here, we used an MEH-PPV OLED designed to have imbalanced injection of majority electron polarons to promote the formation of TEPs consisting of two electrons and one hole[13]. The device was operated at T=10 K.For more information see the supplementary information[18]. In an external magnetic field, B, we apply short bursts of intensive microwave ($\approx$ 9.7GHz) pulses to excite ESR–allowed transitions between the spin eigenstates. The transient changes of the device current $I(t)$ were recorded. The inset of Fig.3a) shows $I(t)$ following a $\tau = 200$ ns pulse as a function of B, similar to that seen in Ref.[13]. Two resonant changes in $I(t)$ are visible around magnetic field values of $B_0 \approx 347$ mT and $B_{1/2} \approx 170$ mT (slightly less than half of B_0). The full–field signal, occurring at magnetic fields corresponding to a Landé–factor of $g \approx 2.002$, is due to both the TEP and the polaron-pair mechanisms[15,19,20]. However, since the TEP and polaron-pair processes have different dynamics, the microwave pulse induced current changes can be distinguished by choosing an appropriate detection time t_m after the excitation pulse[13]. In contrast to the full-field pEDMR signal, the half–field current response is solely governed by the TEP process as polaron-pairs do not have $s = 1$ character. Figure 3a) shows $\Delta I(t)$ after a microwave pulse at $B_{1/2}$. Double exponential dynamics, consistent with theoreti-

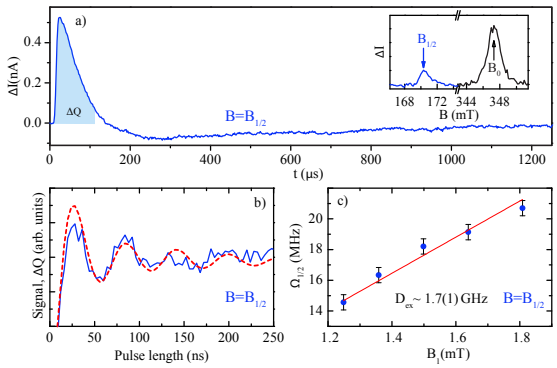

FIG. 3. (a) The change in device current $\Delta I(t)$ following a $\tau = 200$ ns microwave pulse at the $B_{1/2}$ ∼170 mT resonance (The inset shows the full and half-field resonance peaks). The data after the rise time displays good agreement with a bi-exponential decay function known for systems of two competing sub-populations (eg weakly bound exciton-polaron pairs). The shaded blue area indicate the integration interval which provides the signal displayed in (b). (b) The solid line represents the integrated current change, $\Delta Q = \int \Delta(I).dt$, as a function of the applied microwave pulse length recorded at the center of the half–field resonance. The dashed line shows a best fit simulated curve based on a strongly coupled exciton which is weakly coupled to a polaron. The Rabi–oscillation frequency $\Omega_{1/2}$ is extracted from this fit. (c) The data points display Rabi–oscillation frequency $\Omega_{1/2}$ values obtained by fitting experimental data similar to the data set shown in (b) for a number of microwave field strengths B_1. The red line is a linear fit of the blue data points which shows good agreement. The slope of this linear fit provides a measure of the spin–dipolar coupling strength within the exciton $D_{ex} = 1.7(1)$ GHz.

cal modeling[16] and qualitatively similar to the response seen in 2 spin-1/2 systems[21] are seen. This transient shows slower dynamics than the full–field current response which is influenced by both the TEP and the polaron pair dynamics. This observation is consistent with a rate picture based on the dynamics of the polaron pair system (which generates excitons) and the TEP process illustrated in Fig. 1[16].

With the pEDMR detected pure TEP signal at half–field conditions shown in Fig. 3a), we can now study the dynamics of coherent spin motion on a nanosecond timescale by measuring the current transient as a function of the length of the applied microwave pulse [21] as previously reported for $B_{1/2}$ by Ref. 13. The result of this experiment, shown by the blue data in Fig. 3b), reveals a rapidly damped oscillatory behavior caused by the spin–Rabi oscillation of the triplet exciton states. We have developed a fit procedure for this data based on the simulation of the TEP system using a spin–Liouville equation based on a pair Hamiltonian for a s=1/2 and an s=1 spin, containing all relevant exchange and dipolar interactions discussed above. The approach follows similar previous treatments of pairs of two spins with s=1/2[21,22]. Details of the simulations can be found in the Supplementary Information[18]. The simulated spin–Rabi oscillation driven changes in integrated charge, ΔQ, shown in Fig. 3b) show good agreement with the experimental data when appropriate simulation parameters (e.g. the coupling strengths) are chosen.

Figure 3b) shows that exciton-polaron complexes can be resonantly controlled with microwaves and this can be used to study the dynamics of coherent TEP spin–motion. The resonance signal observed at $B_{1/2}$ is predominantly due to triplet–exciton spin transitions with $\Delta m = \pm 1$ [transitions 3-6 and 4-8 in Fig. 2a)]. These transitions have previously been studied with both EDMR and optically-detected magnetic resonance (ODMR) experiments[13,23,24], but only with continuous wave (cw) experiments which did not not allow the observation of coherent spin motion. The remainder of this work will focus on the information that can be extracted by examining coherent effects.

The existence of the excitonic $\Delta m = \pm 1$ half–field resonance provides the first indication of a dipolar interaction within the exciton, as spin–dipolar interactions introduce off-diagonal elements that mix the T_- and T_+ states. This produces a small but non-negligible ESR–transition probability for these otherwise forbidden transitions[25]. Due to the reduced magnitude of the static field, the commonly used rotating wave approximation is no longer valid[26]. This was simulated using a second order expansion of the time-averaged Hamiltonian. This revealed a half-field Rabi oscillation frequency $\Omega_{1/2} \propto \frac{B_1 D_{ex}}{B_0} \sin(2\theta)$ in which the angle θ represents the orientation of the laboratory frame (governed by the external magnetic field orientation) with regard to the molecular frame of the triplet state[16,2718] . The measured TEP spin–Rabi oscillation frequency can therefore be used to quantify the exciton dipolar interaction strength D_{ex}. To do this, we have repeated the measurements of the resonantly induced spin–Rabi oscillation at half–field conditions for various driving fields B_1[28]. The results of these measurements were fit in the same way as the data shown in Fig. 3b). The nutation frequencies $\Omega_{1/2}$ obtained are plotted in Fig. 3c) as a function of B_1. This plot shows a good agreement with a linear fit function from which we obtain a dipolar interaction strength within the exciton of $D_{ex} = 1.7(1)$GHz. This result matches previously determined values for the exciton zero-field parameters in PPV blends[29], providing support for the model.

The model also allows us to determine the intrapair–exchange between the triplet exciton and the polaron from the full–field spin–Rabi oscillation measurement. Figure 4 a) (black curve) displays the spin–Rabi oscillation reflected by the integrated device current, ΔQ, after the application of a resonant microwave pulse at B_0 as a function of pulse duration. This corresponds to the rotation of the polaron s=1/2 particle within the complex with a Rabi-frequency of $\gamma_e B_1$, where B_1 is the magnitude of the oscillating field and γ_e the gyromagnetic ratio[30]. The observed signal is caused by transitions 4-3 and 7-8 in Fig.2a), leading to an increase in polaron mobility and thus, an increase in current. The spin–Rabi oscillation seen in Fig. 4a) was recorded at B_0 with the same microwave frequency as the data in Fig. 3b). While the oscillation at the half–field condition is caused by spin–Rabi oscillation of the exciton, the observation at the full–field condition is due to the polaron spin–Rabi oscillation.

The TEP model explains the occurrence and frequency of the oscillation of both the full- and half–field pEDMR signals. At full field, the excitation is resonant with both polaronic (transitions 6-8 and 4-3) and excitonic (4-7 and 5-6)

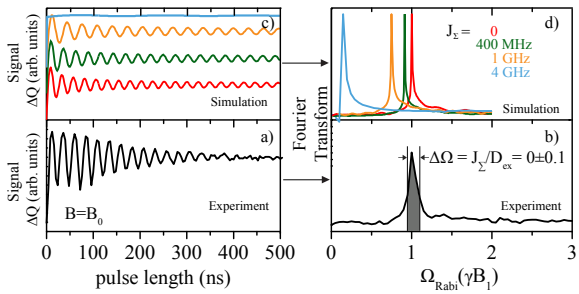

FIG. 4. (a) Plot of the integrated current change ΔQ as a function of the applied microwave pulse length recorded at the center of the full–field resonance. (b) Fourier transform of the experimental data displayed in (a) with a frequency scale in units of γB_1 with γ being the gyromagnetic ratio. (c) Simulated values of ΔQ with J_Σ corresponding to 0 (red), 400 MHz (green), 1 GHz (orange) and 4 GHz (light blue). (d) The normalised Fourier-transform of the simulated data displayed in (c) with a frequency scale in units of γB_1. The comparison of the experimentally obtained spin–Rabi frequency distribution with the simulated data sets shows that the best agreement is obtained for $J_\Sigma = 0 \pm 170$MHz. The error in the full-width half-maximum (FWHM) of the fast Fourier transform (FFT) in (b) sets an upper bound on J_Σ.

transitions(see Fig. 2). However, transitions 6-8 and 4-3 will dominate the signal due to the high quartet-content ($s = 3/2$) of the steady state. For prolonged coherent excitation over several Rabi-periods, our calculations show that it is possible to observe beating between the polaronic and excitonic transitions. However, due to the low exciton–nutation frequency, only the contribution from the polaronic nutation provides a significant signal. This results in the observation of spin–Rabi oscillation with a frequency corresponding solely to that of a single polaron ($s = 1/2$).

As we adjust the interaction strengths between the exciton and polaron, $J_\Sigma = J_1 + J_2$, the energy levels of the corresponding energy eigenstates are modified, changing the expected frequency of Rabi-oscillation at full-field, $\Delta\Omega = -\gamma B_1 J_\Sigma / D_{ex}$. This dependence of $\Delta\Omega$ on J_Σ, along with D_{ex} obtained from the half-field resonance, can be used to quantify the spin-coupling strength between the exciton and polaron. Figure 4(c) shows simulations[18] of the expected full-field signal for various values of J_Σ. Figure 4(d) displays the frequency components of the data in Fig.4(c). The Fourier transform of the experimental data in Fig. 4(b) shows good agreement with simulations with $J_\Sigma \leq 170$MHz. Thus, an upper bound of 0.7μeV can be placed for the triplet–exciton polaron spin-coupling strength, 5 to 6 orders of magnitude weaker than the excitonic exchange. Since the anisotropic nature of the dipolar coupling effect would cause a broadening of the Rabi frequency distribution[31], an upper bound of 5 MHz based on the width of the peak in Fig. 4(b) is also obtained.

In conclusion, we compare the influence of magnetic resonantly induced spin–motion of TEPs on the current of MEH-PPV diodes with calculations based on the TEP model, revealing strong intra-exciton dipole coupling ($D_{ex} = 1.7(1)$ GHz) and weak exciton–polaron exchange ($J_\Sigma \leq 170$ MHz) and dipolar (< 5 MHz) couplings. This allows us to discount other possible coupling regimes, such as trion states, which consists of three strongly coupled charges[11]. By providing a probe which can be widely applied to directly measure the microscopic coupling properties of multi-spin complexes, the experimental approach and theoretical framework described here significantly advances our ability to validate hypotheses linking microscopic properties with bulk magneto-conductive and magneto-optical characteristics of organic electronic devices.

ACKNOWLEDGMENTS

We acknowledge support from the Australian Research Council (DP12102888). DRM is supported by an ARC Future Fellowship (FT130100214) and TK by the Australian Renewable Energy Agency. The experimental data presented in this study was measured with support by the U.S. Department of Energy, Office of Basic Energy Sciences, Division of Material Sciences and Engineering under Award DE-SC0000909.

* dane.mccamey@unsw.edu.au

[1] K. Ando, S. Watanabe, S. Mooser, E. Saitoh, and H. Sirringhaus, Nat Mater **12**, 622 (2013).
[2] A. Rao, P. C. Y. Chow, S. Gelinas, C. W. Schlenker, C.-Z. Li, H.-L. Yip, A. K.-Y. Jen, D. S. Ginger, and R. H. Friend, Nature **500**, 435 (2013).
[3] M. Warner, S. Din, I. S. Tupitsyn, G. W. Morley, A. M. Stoneham, J. A. Gardener, Z. Wu, A. J. Fisher, S. Heutz, C. W. M. Kay, and G. Aeppli, Nature **503**, 504 (2013).
[4] C. Boehme and J. M. Lupton, Nat Nano **8**, 612 (2013).
[5] C. Boehme, D. R. McCamey, K. J. van Schooten, W. J. Baker, S.-Y. Lee, S.-Y. Paik, and J. M. Lupton, phys. stat. sol. (b) **246**, 2750 (2009).
[6] D. R. McCamey, K. J. van Schooten, W. J. Baker, S.-Y. Lee, S.-Y. Paik, J. M. Lupton, and C. Boehme, Phys. Rev. Lett. **104**, 017601 (2010).
[7] H. Malissa, M. Kavand, D. P. Waters, K. J. van Schooten, P. L. Burn, Z. V. Vardeny, B. Saam, J. M. Lupton, and C. Boehme, Science **345**, 1487 (2014).
[8] P. Janssen, M. Cox, S. Wouters, M. Kemerink, M. Wienk, and B. Koopmans, Nat Commun **4**, (2013).
[9] P. Desai, P. Shakya, T. Kreouzis, W. P. Gillin, N. A. Morley, and M. R. J. Gibbs, Phys. Rev. B **75**, 094423 (2007).
[10] M. Cox, E. H. M. van der Heijden, P. Janssen, and B. Koopmans, Phys. Rev. B **89**, 085201 (2014).
[11] M. Cox, P. Janssen, F. Zhu, and B. Koopmans, Phys. Rev. B **88**, 035202 (2013).
[12] D. R. McCamey, H. Huebl, M. S. Brandt, W. D. Hutchison, J. C. McCallum, R. G. Clark, and A. R. Hamilton, Appl. Phys. Lett. **89**, 182115 (2006).
[13] W. J. Baker, D. R. McCamey, K. J. van Schooten, J. M. Lupton, and C. Boehme, Phys. Rev. B **84**, 165205 (2011).

[14] E. L. Frankevich, A. A. Lymarev, I. Sokolik, F. E. Karasz, S. Blumstengel, R. H. Baughman, and H. H. Horhold, Phys. Rev. B **46**, 9320 (1992).
[15] D. R. McCamey, H. A. Seipel, S.-Y. Paik, M. J. Walter, N. J. Borys, J. M. Lupton, and C. Boehme, Nat Mater **7**, 723 (2008).
[16] T. L. Keevers, W. J. Baker, C. Boehme, and D. R. McCamey, arXiv:1502.05470 (2015).
[17] M. Reufer, M. J. Walter, P. G. Lagoudakis, A. B. Hummel, J. S. Kolb, H. G. Roskos, U. Scherf, and J. M. Lupton, Nat Mater **4**, 340 (2005).
[18] "Supplementary information can be found at insert link,".
[19] W. Baker, K. Ambal, D. Waters, R. Baarda, H. Morishita, K. van Schooten, D. McCamey, J. Lupton, and C. Boehme, Nat. Communications **3**, 898 (2012).
[20] W. J. Baker, T. L. Keevers, J. M. Lupton, D. R. McCamey, and C. Boehme, Phys. Rev. Lett. **108**, 267601 (2012).
[21] C. Boehme and K. Lips, Phys. Rev. B **68**, 245105 (2003).
[22] P. A. Bobbert, T. D. Nguyen, F. W. A. van Oost, B. Koopmans, and M. Wohlgenannt, Phys. Rev. Lett. **99**, 216801 (2007).
[23] C. Kollmar and H. Sixl, Mol. Phys. **45**, 1199 (1982).
[24] L. S. Swanson, J. Shinar, A. R. Brown, D. D. C. Bradley, R. H. Friend, P. L. Burn, A. Kraft, and A. B. Holmes, Phys. Rev. B **46**, 15072 (1992).
[25] J. Van der Waals and M. De Groot, Molecular Physics **2**, 333 (1959).
[26] C. P. Slichter, *Principles of Magnetic Resonance*, third edition ed. (Springer, New York, 1989).
[27] A. Abragam and B. Bleaney, *Electron paramagnetic resonance of transition ions* (Oxford University Press, Oxford, 2012).
[28] B_1 was calibrated by measuring the Rabi oscillation frequency of the polaron-pair signal at full field.
[29] L. S. Swanson, J. Shinar, and K. Yoshino, Phys. Rev. Lett. **65**, 1140 (1990).
[30] A. Schweiger and G. Jeschke, *Principles of pulse electron paramagnetic resonance* (Oxford University Press, Oxford, 2001).
[31] S.-Y. Lee, S.-Y. Paik, D. McCamey, J. Hu, F. Zhu, A. Madan, and C. Boehme, Appl. Phys. Lett. **97**, 192104 (2010).